Diffusion measured by fluorescence recovery after photobleaching based on multiphoton excitation laser scanning microscopy

Edrun Andrea Schnell
Live Eikenes
Ingunn Tufto
Arne Erikson
Aphirak Juthajan
Mikael Lindgren
Catharina de Lange Davies
The Norwegian University of Science and Technology
Department of Physics
7491 Trondheim, Norway

Abstract. Fluorescence recovery after photobleaching (FRAP) is a widely used method to measure diffusion. The technique is normally based on one-photon excitation, which limits diffusion to two dimensions due to extended photobleaching in the axial direction. Multiphoton excitation, on the other hand, creates a well-defined focal volume. In the present work, FRAP based on a scanning laser beam and two-photon excitation is used to measure diffusion of macromolecules in solution and gels, as well as in the extracellular matrix in multicellular spheroids and tumor tissue in dorsal chambers. The bleaching profile is determined experimentally in immobilized gels, and for small scanning areas (approximately twice the lateral radius of the laser beam) a Gaussian bleaching distribution is found. In addition, the bleaching profile is determined theoretically based on the convolution of the Gaussian point spread function and a circular scanning area. The diffusion coefficient is determined by fitting a mathematical model based on a Gaussian laser beam profile to the experimental recovery curve. The diffusion coefficient decreases with increasing complexity of the sample matrix and increasing the amount of collagen in the gels. The potential of using two-photon laser scanning microscopes for noninvasive diffusion measurements in tissue is demonstrated.
[DOI: 10.1117/1.3042274]

Keywords: fluorescence recovery after photobleaching; interstitial diffusion; mobile fraction; multicellular spheroids; tumor tissue.

Paper 08011RR received Jan. 11, 2008; revised manuscript received Oct. 15, 2008; accepted for publication Oct. 29, 2008; published online Dec. 19, 2008.

1 Introduction

Diffusion is a fundamental physical transport process in tissue. Transport of molecules in cytosol, in membranes as well as in the extracellular matrix, is governed by diffusion. Intracellular diffusion of various molecules is crucial for cellular functions, and extracellular diffusion is the main transport mechanism for oxygen, nutrition, and small regulatory and therapeutic molecules. Thus, the development of techniques for noninvasive *in-situ* measurements of diffusion is of great importance.

Fluorescence recovery after photobleaching (FRAP) is a widely used method to measure translational diffusion.[1] The technique is normally based on one-photon excitation and bleaching of fluorophore-labeled molecules using a high-intensity laser beam. The bleached area is monitored using a laser with attenuated intensity, and from the recovery of fluorescence into the bleached area the diffusion coefficient can be estimated. FRAP using one-photon excitation has been limited to diffusion in two dimensions (2-D), because the focused laser beam generates extended photobleaching in the axial direction above and below the focal plane. 3-D models using low numerical aperture objectives and one-photon stationary or scanning laser excitation have been developed.[2–4] However, such models are based on extensive numerical calculations, and a major problem is that the bleaching distribution in the axial direction depends on the sample thickness, which usually is hard to define accurately. Multiphoton excitation, on the other hand, creates a well-defined focal volume, and bleaching occurs only in the focal plane.[5] FRAP based on multiphoton excitation may therefore be used for accurate measurements of 3-D diffusion, and has been developed using a stationary laser beam.[6–10]

Confocal laser scanning microscopes (CLSM) equipped with multiphoton excitation lasers are becoming standard instrumentation in many laboratories and core facilities, and can be used for 3-D diffusion measurements. However, some commercial CLSMs have too slow image acquisition rates for accurate diffusion measurements of small molecules in solution. This becomes a major problem when parking the laser beam, and due to the fast diffusion, the recovery may not be recorded. Increasing the effective recovery time by increasing

Address all correspondence to: Catharina de Lange Davies, The Norwegian University of Science and Technology, Dept of Physics, Høgskoleringen 4, 7491 Trondheim, Norway. Tel: +47 73593688, Fax: +47 73597710, E-mail: catharina.davies@phys.ntnu.no.

1083-3668/2008/13(6)/064037/12/$25.00 © 2008 SPIE

the size of the bleached area may overcome this problem,[11] although caution should be taken if diffusion occurs during the bleaching process. Scanning a larger region of interest (ROI) also improves the signal-to-noise ratio. Another advantage of using a scanning laser beam is that any arbitrary shaped region can be bleached. The purpose of the present work was thus to extend FRAP based on multiphoton excitation and a stationary laser beam to a scanning laser beam.

By using a stationary laser beam, the bleached volume is well defined by the Gaussian laser beam, and the diffusion coefficient can be calculated based on the mathematical model developed by Brown et al.[6] When applying a scanning laser beam, a theoretical estimation of the bleached volume is based on the convolution of the point spread function (PSF) of the laser beam and the scan area. The bleaching profile will, however, depend on several parameters such as the optical components, scanning process, refractive indices, and the intensity and wavelength of the laser. In the present work the bleached volume was determined using a semiempirical approach, and the axial and radial bleaching radii were determined experimentally for various diameters of the bleached ROI. In addition, the bleaching profile was calculated theoretically based on the convolution product between the Gaussian PSF and a circular scanning area of various radii. We wanted to apply a simple mathematical model describing the bleaching and recovery processes, as such a model could be adapted by more users. The model developed by Brown et al.[6] for a stationary laser was therefore used, and the appropriate scanning criteria for using this model were determined. The diffusion coefficients were determined for high molecular weight molecules in solution and gels as well as in the extracellular matrix in multicellular spheroids and in tumor tissue in dorsal chambers. The potential of using a commercially or laboratory built CLSM equipped with multiphoton laser excitation for noninvasive measurements of diffusion in tissue *in vivo* is demonstrated. This is to our knowledge the first time FRAP based on scanning multiphoton excitation has been used to measure 3-D diffusion in tumor tissue *in vivo*.

2 Materials and Methods

2.1 *Two-Photon Laser Scanning Microscopy and Fluorescence Recovery after Photobleaching*

FRAP experiments and imaging were performed using an LSM 510 confocal scanning microscope (Carl Zeiss, Jena, Germany) with a C-Apochromat 40×/1.2 water immersion (W) objective and a C-Achroplan 40×/0.8 W objective. The laser source was a Mira Model 900-F mode-locked Ti:sapphire laser (Coherent, Incorporated, Santa Clara, California) pumped by a solid-state Verdi V-5 laser at 532 nm (Coherent, Incorporated). The Ti:sapphire laser produces 200-fs pulses with a repetition rate of 76 MHz, and at 780-nm excitation the output power was 800 mW at the laser cavity and 40 or 20 mW at the objective for the C-Apochromat 40×/1.2 W and C-Achroplan 40×/0.8 W, respectively. Fluorescein isothiocyanate (FITC) was excited at 780 nm, and the fluorescence was detected using a bandpass 500- to 550-nm filter. The laser power was attenuated to 5% of the 100% bleach intensity by an acousto-optical modulator, to minimize bleaching and avoid saturation of the detector during imaging.

Each FRAP experiment started with ten image scans of the user-defined ROI, followed by a bleach pulse. The bleached ROI in the *xy* plane was circular with a radius of 8, 12, or 16 pixels corresponding to 1.8, 2.7, or 3.6 μm, respectively. Each ROI was bleached using maximum laser power, maximum scanning speed, and ten scanning iterations in a raster scan across the ROI. This corresponded to a total bleach scanning time for the three ROIs of 75, 115, and 150 ms, respectively. The total bleach scanning time is the time from bleach start to end, which includes the actual bleaching time per pixel (1.6 μs/pixel×10 iterations) and the time needed for repositioning of the laser to the next line of pixels. The bleach scanning time used was the shortest period that achieved maximum bleaching (difference between prebleached and postbleached intensity divided by prebleached intensity) of FITC-dextrans (Sigma-Aldrich, Saint Louis, Missouri) in spheroids.

To determine the recovery curve, series of up to 600 images of the bleached ROI were collected at the highest possible rate. Only the bleached ROI was imaged. For the three ROI sizes used, this corresponded respectively to 11.6, 17.4, and 25.1 ms per image (duration of the acquisition of the image of one ROI plus the shortest possible time between each acquisition, which was 0.1 ms). The fluorescence intensity of the bleached ROI was determined as the average pixel value, and normalized to the average fluorescence intensity after reaching a stable level. The normalized recovery curves were fitted to estimate the diffusion coefficient (D), the mobile fraction (R_{mob}), and the bleaching parameter (β), as described next.

A high numerical objective 40×/1.2 W was used in all experiments except for measurements in dorsal window chambers. These chambers required an objective with a long working distance, and here the C-Achroplan 40×/0.8 W objective was used. When performing FRAP experiments with this objective combined with tumors growing in dorsal window chambers, the image had to be magnified to decrease the pixel size to obtain sufficient laser intensity per pixel. The images were zoomed to pixel size 0.11 μm. In all other experiments the pixel size was 0.45 μm and the image size 512×512 pixels. To ensure that the zooming did not affect the measured diffusion coefficient, the diffusion coefficient of 150-kDa FITC-dextrans in solution was determined for pixel sizes 0.45 and 0.11 μm, and found to be the same (data not shown).

To ensure that no excitation saturation took place during bleaching, the bleach depth parameter (β) for 2-MDa FITC-dextran molecules in solution was measured as a function of laser power using the 40×/1.2 objective. The bleaching and scanning of an ROI with radius 2.7 μm was performed as described before. To further ensure that a two-photon bleaching process took place, the fluorescence intensity of 2-MDa dextran molecules (1 mg/ml) immobilized in a 15% polyacrylamide gel was measured as a function of laser exposure time and bleaching laser power. The fluorescence intensity was measured as the average pixel value in an ROI with radius 1.8 μm. The gels were made from a mixture of acrylamide (Sigma-Aldrich) and bisacrylamide (Bio-Rad Laboratories, Richmond, California) in the ratio 37.5:1 with 0.5% ammonium persulphate (Sigma-Aldrich) and 5% aqueous N,

N, N′, N′-tetramethylethylenediamine (Sigma-Aldrich) as polymerization catalysts. The biexponential decay function $[I(t)=ae^{-bt}+ce^{-dt}]$ was fitted to the measured fluorescence intensity to determine the bleaching rate. The bleaching rate b was much larger than d, thus b was used as the bleaching rate.

2.2 *Experimental Bleaching Profiles*

The bleaching profiles were determined experimentally using FITC-labeled dextrans with average molecular weights of 500 kDa or 2 MDa immobilized in a 15% polyacrylamide gel to a final concentration of 1 mg/ml. The gels were prepared as described before. Bleaching was performed using the scanning conditions described before.

The radial bleaching profile when using a stationary laser beam was determined by parking the laser beam and generating the bleaching profile in the xy plane. The axial bleaching profile could not be obtained. The bleaching profiles when scanning the laser beam were generated for the three ROIs in both the radial and axial directions. To determine the axial bleaching profile, a z stack of the bleached area was acquired, and the number of consecutive confocal images and distance between each image necessary to cover the bleached axial area were used, which corresponded to 20 consecutive images with a distance of 0.74 μm. Ten independent xy images and z stacks were acquired for each ROI to determine the average bleaching radial (ω_r) and axial (ω_z) radius, respectively, and the bleaching radii were determined as described next (theory: the FRAP analysis model). The bleaching radii were determined for both objectives used.

To determine if there was any diffusion during bleaching, an image was taken of the bleached ROI immediately (0.1 ms) after the bleach scan using a solution of 150-kDa, 500-kDa, and 2-MDa FITC-dextran. Radial profiles of the bleached area were made and compared to the profiles from the experiments using immobilized gels. Assuming that no diffusion occurred during bleaching, the bleaching profiles for the dextrans in solution and in immobilized gel should be the same.

2.3 *Sample Preparation for Diffusion Measurements*

Diffusion was measured for FITC-labeled dextran molecules of size 40 kDa, 150 kDa, 500 kDa, 2 MDa, and IgG (Sigma-Aldrich), either in solution [phosphate buffered saline (PBS)], in gelatin or collagen gel, or in tumor tissue growing as multicellular spheroids or in dorsal window chambers.

Gelatin gels were prepared from bovine gelatin powder (Kebo, Oslo, Norway) dissolved in PBS to 5% and incubated at 45 °C for at least 20 min. FITC-dextrans were added to the aqueous hydrogel to obtain a homogenous distribution before cooling to room temperature.

Collagen gels were prepared using Vitrogen 100 collagen type-1 solution (Cohesion Technologies, Palo Alto, California) as described previously.[12] In brief, the pH and ionic strength were adjusted by addition of NaOH to pH 7.4 and 10× PBS. To concentrate the solution, the collagen was ultracentrifuged (Optima LE-80K Ultrasentrifuge, Beckman Coulter, Fullerton, California) at 5 °C for 24 to 60 h to obtain ~1 to 2% gels. The collagen concentration in the pellet was determined by UV spectrophotometry by determining the difference in collagen content of the solution before ultracentrifugation and in the supernatant afterward.

Multicellular spheroids were made from the human osteosarcoma cell line OHS.[13] Briefly, $2\cdot10^6$ cells were seeded in 80-cm^2 tissue culture flasks (Nunc, Tamro AS, Skårer, Norway) precoated with 1% agar to prevent cell attachment, and containing 25-ml growth medium [RPMI-1640 supplemented with 10% fetal bovine serum, 100-units/ml penicillin/streptomycin, and 1-mM L-glutamine (all from Sigma-Aldrich)], and kept at 37 °C and 5% CO_2. Half of the medium was changed twice a week. Spheroids were harvested for experiments after 5 to 6 days, when their diameter had reached 150 to 250 μm.

Transparent window skinfold chambers were implanted on the back of athymic BALB/c nu/nu mice (10 to 16 weeks old, 24 to 27 g, Taconic, M&B, Ry, Denmark) as described by Endrich et al.[14] Briefly, an extended double layer of skin was sandwiched between two symmetrical titanium frames, and a circular area of 15 mm in diameter was removed from one layer of skin. The remaining layers of the other skin fold (thin striated skin muscle, subcutaneous tissue, dermis, and epidermis) were covered with a glass coverslip incorporated into one of the titanium frames. 24 h after the implantation of the chamber, the coverslip was removed and $1.5\cdot10^6$ OHS cells were placed into the center of the chamber. A new glass coverslip was replaced and the chamber closed. All surgical procedures were performed under sterile conditions, and the mice were anesthetized by i.p. injection of Fentanyl/Midazolam/Halsol/sterile water (3:3:2:4) in the amount of 12-ml/kg body weight (Hameln Pharmaceuticals, Germany, Alpharma AS, Norway, and Janssen-Cilag AS, Norway). The animals were kept under pathogen-free conditions at constant temperature (24 to 26 °C) and humidity (30 to 50%), and were allowed food and water *ad libitum*. All animal experiments were carried out with ethical committee approval.

FITC-dextran molecules were mixed with PBS or the gel to a concentration of 1 mg/ml. Multicellular spheroids were incubated with 1-mg/ml FITC-dextrans for 6 h on a roller at 37 °C before measuring diffusion. Athymic mice received 200-μl i.v. injections in the tail vein of 20-mg/ml 150-kDa FITC-dextrans 24 before measuring diffusion. Tetramethyl rhodamine-dextran 580 kDa (Invitrogen, Eugene, Origon) was injected $i.v.$ (200 μl of 10 mg/ml) to visualize the blood vessels.

2.4 *Statistical Analyses and Fitting Routine*

Two-sample two-tailed student's t tests assuming nonequal variances were applied to the Gaussian distributed data to compare population means (Minitab, Minitab Incorporated, State College, Pennsylvania). All statistical analyses were performed using the significance criterion of $p \leq 0.05$.

Fitting was performed using the Matlab 7.0 lsqcurvefit function (The Math Works, Natick, Massachusetts), and the results plotted using the SigmaPlot 9.0 software (Systat Software, Incorporated, Richmond, California).

3 Theory: Fluorescence Recovery after Photobleaching Analysis Model

3.1 *Theoretical Bleaching Profile*

The theoretical bleaching profile can be described by the bleaching light distribution $B(r,\theta)$, which is given as a convolution of the laser beam PSF and the 2-D circular scanning area. The laser beam profile is assumed to be Gaussian in both the radial and axial directions:

$$I^b(r,z) = I_0^b \exp(-2br^2/\omega_r^2 - 2bz^2/\omega_z^2), \tag{1}$$

where $b=2$ for two-photon excitation, and ω_r and ω_z are the $1/e^2$ radial and axial dimensions, respectively.

The two-dimensional radial convolution product in the scanning plane is obtained by integrating over the circular scanning area of radius R and all angles, and gives the bleaching light distribution:

$$\begin{aligned} B(r,\theta) &= \int_0^{2\pi}\int_0^R I^2(|\mathbf{r}-\mathbf{r}'|)r'dr'd\theta \\ &= \int_0^{2\pi}\int_0^R I_0^2 \exp(-4(|\mathbf{r}-\mathbf{r}'|^2)/\omega_r^2)r'dr'd\theta \\ &= I_0^2 \exp(-4r^2/\omega_r^2)\left\{\int_0^R \exp(-4r'^2/\omega_r^2)r' \right. \\ &\times \left.\left[\int_0^{2\pi} \exp(8rr'\cos\theta/\omega_r^2)d\theta\right]dr'\right\}, \end{aligned} \tag{2}$$

$$= \frac{2}{\pi} I_0^2 \exp(-4r^2/\omega_r^2)\int_0^R r' \exp(-4r'^2/\omega_r^2)dr' J_0(8rr'/\omega_r^2), \tag{3}$$

where $\mathbf{r}$ is the position of the bleached point, $\mathbf{r}'$ is the position of the laser beam, and θ is the angle between the two vectors $\mathbf{r}$ and $\mathbf{r}'$. J_o is the Bessel function. Equation (3) shows that for small R, the bleaching light distribution is dominated by the Gaussian function. Equation (2) was plotted for various scanning radii R and $\omega_r=1$ μm using Maple (MapleSoft, Waterloo, Canada), and is shown in Fig. 1. The radius of the laser beam was chosen to $\omega_r=1$ μm because the bleaching profile using a stationary laser beam had a radius $\omega_r=1$ μm at $1/e^2$ intensity (Fig. 1), i.e., the Gaussian laser beam profile was assumed to be equal to the bleaching profile of a stationary laser beam.

3.2 *Determination of Radial and Axial Bleaching Radii*

The actual bleaching profile obtained when using a laser scanning microscope will not be exactly described by the bleach light distribution.[2] The bleaching profile was thus determined experimentally using immobilized FITC-labeled dextran molecules in a polyacrylamide gel, as described earlier. The axial and radial bleaching radii were determined by fitting the expression for the concentration of unbleached molecules in the circular area of interest [Eq. (5)] to the experimental

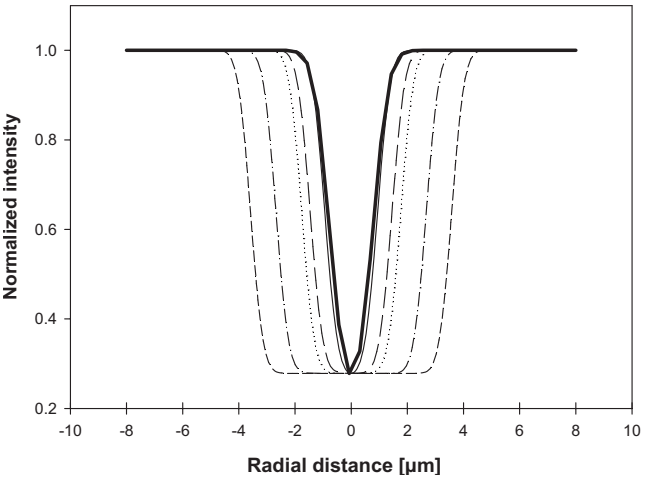

Fig. 1 Simulation of bleaching light distribution from Eq. (2). The Gaussian laser beam profile is integrated over a circular ROI with radius $R=1.0$ μm (—), $R=1.5$ μm (——), $R=1.8$ μm (···), $R=2.7$ μm (–·–), and $R=3.6$ μm (---). The bold solid line represents the bleaching profile when parking the laser beam.

bleaching profile, according to Braga, Desterro, and Carmo-Fonseca.[4] The photo-bleaching process was assumed to follow a first-order differential equation:

$$dC(r,z,t)/dt = -(1/b)q_b\delta_b I^b(r,z)C(r,z,t), \tag{4}$$

where b is the order of bleaching, δ_b is the absorption cross section of the fluorophore being bleached, and q_b is the quantum efficiency for two-photon bleaching. This requires that there is no saturation in the excitation process. $I^b(r,z)$ represents the 3-D Gaussian distribution of the laser intensity given by Eq. (1).

Assuming two-photon excitation ($m=2$) and bleaching ($b=2$), the solution to the differential in Eq. (4) is expressed as:

$$C(r,z) = C_0 \exp(-\beta \exp\{-4[(r-r_o)^2/\omega_1^2] - 4[(z-z_o)^2/\omega_2^2]\}), \tag{5}$$

where C_0 is the initial concentration of fluorophores, ω_1 and ω_2 are characteristic parameters related to the width of the bleaching profile in radial and axial directions, respectively, and r_0 and z_0 are fitting parameters to define the zero-position corresponding to the center point of our experimental data. β is the bleach depth parameter given by:

$$\beta = (1/b)q_b\delta_b I_o^b \Delta t, \tag{6}$$

where Δt is the duration of the bleach pulse. The radial and axial bleaching radii are considered to be independent, and in the fitting, Eq. (5) was separated into the axial and radial part. The parameter C_0 was set to unity, since the bleached region was normalized to the fluorescence signal prior to the analysis. The axial part was first fitted using data from the z-stack images using β_z, ω_2, and z_0 as free parameters. β_r, ω_1, and r_0 were subsequently fitted by using the dataset corresponding to $z=0$. β_r and β_z were found to be almost the same. Assuming a Gaussian laser bleaching profile, the $1/e^2$ radial and axial

radii were determined by solving Eq. (5) for $r=\omega_r$ and $z=\omega_z$. For larger ROIs ($\geq$12 pixels), the radial part was fitted using a product of two independent Gaussian bleaching profiles separated a distance $2\omega_s$. Together they defined a total $1/e^2$ radial width of $\omega_r'+\omega_s$.

3.3 *Determination of Diffusion Coefficient and Bleaching Parameter*

The equation describing the recovery of fluorescence into the area bleached by a stationary one- and two-photon laser has been developed by Axelrod et al.[1] and Brown et al.,[6] respectively. We found that two-photon laser scanning over a small circular area generated a bleaching profile well fitted by an exponential of a Gaussian [Eq. (5)], i.e., the bleaching profile generated by an idealized stationary Gaussian laser beam (see Sec. 4). Assuming a Gaussian bleaching profile, the recovery curve can be fitted to the following equation from Brown et al.,[6] including the mobile fraction $R_{\mathrm{mob}}=[F_\infty-F(0)]/[F_0-F(0)]$:

$$\frac{F(t)}{F_\infty}=1-\frac{F_\infty-F(0)}{F_0-F(0)}\times\left(1-\sum_{n=0}^{\infty}\frac{m^{3/2}(-\beta)^n}{n!}\frac{1}{[m+bn+(bnmt/\tau_D)]}\times\frac{1}{\{m+bn+[bnmt/(\omega_z^2/\omega_r^2)\tau_D]\}^{1/2}}\right). \quad (7)$$

This equation is valid for a single freely diffusing species in three dimensions and is generalized for the m'th photon excitation and the b'th photon bleaching. Here, F_0 is the prebleach intensity, $F(0)$ the intensity at time $t=0$ after bleaching, and F_∞ the intensity of the bleached spot at infinite time after bleaching. β represents the bleaching parameter. For two-photon excitation and two-photon bleaching, and with the characteristic radial diffusion time $\tau_D=\omega_r^2/8D$, Eq. (7) yields:

$$\frac{F(t)}{F_\infty}=1-\frac{F_\infty-F(0)}{F_0-F(0)}\times\left(1-\sum_{n=0}^{\infty}\frac{(-\beta)^n}{n!}\frac{1}{\{1+n[1+(16Dt/\omega_r^2)]\}}\times\frac{1}{\{1+n[1+(16Dt/\omega_z^2)]\}^{1/2}}\right). \quad (8)$$

D is the diffusion coefficient of the fluorophore, and ω_r and ω_z are the radial and axial $1/e^2$ radii of the bleached area, respectively. D and β were determined by fitting Eq. (8) to the experimental recovery curve. The series expansion typically was summed up to $n=7$; extending the summation did not change the fit. Equation (8) is based on a Gaussian bleaching profile. However, we also investigated if reliable diffusion coefficients could be obtained by fitting Eq. (8) to recovery curves based on non-Gaussian bleaching profiles, which were generated by scanning the laser across larger ROIs. The experimentally determined ω_r and ω_z for such bleaching profiles were inserted in Eq. (8).

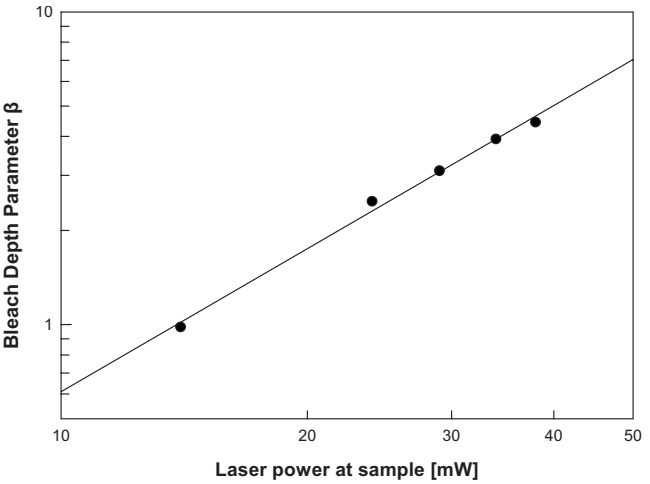

Fig. 2 The bleach depth parameter β as a function of laser power for 2-MDa FITC-dextrans in solution. The linear relationship demonstrates that there is no excitation saturation during bleaching.

4 Results

4.1 *Excitation and Bleaching Processes*

The FRAP analysis is based on the assumption that there is no excitation saturation during bleaching. The linear relation in Fig. 2 demonstrates that this was the case. From the bleaching rate one may estimate the "multiplicity" of the excitation process, i.e., two-photon, three-photon, mixed variants, etc. The bleaching decay and corresponding bleach rate as a function of laser power is shown in Fig. 3. The slope of this log-log plot was 2.1, demonstrating a two-photon bleaching process as described by Patterson and Piston.[15]

4.2 *Theoretical Bleaching Profiles*

The bleaching profile when parking the two-photon laser beam was determined experimentally using FITC-dextran molecules in an immobilized gel. β was found to be $\beta=0.68\pm0.04$, and the $1/e^2$ radius $\omega_r=0.98\pm0.23$ μm (bold line in Fig. 1). This radius is approximately three times wider than the theoretical laser beam radius of 0.32 μm given by Williams, Piston, and Webb.[16] In the simulations, the radius of the laser was chosen to be $\omega_r=1$ μm.

The theoretical bleaching profile based on the convolution product of the PSF and a circular scanning area of various radii are shown in Fig. 1. A Gaussian bleaching profile was obtained when the scanning radius R was equal to the $1/e^2$ radius of the laser beam. The bleaching profile became broader and the discrepancy from the Gaussian profile increased with increasing bleaching radius. For large R, the bleaching profile can be characterized by the uniform disk model described by Braeckmans et al.,[3] where the intensity profile was approximated by a discontinuous step function, which was one inside the bleaching disk and zero outside.

4.3 *Experimental Bleaching Profiles*

Experimentally obtained bleaching profiles will not be exactly described by the convolution product since the laser beam has to pass various optical components and was therefore measured for three different scanning radii (Fig. 4). For a small

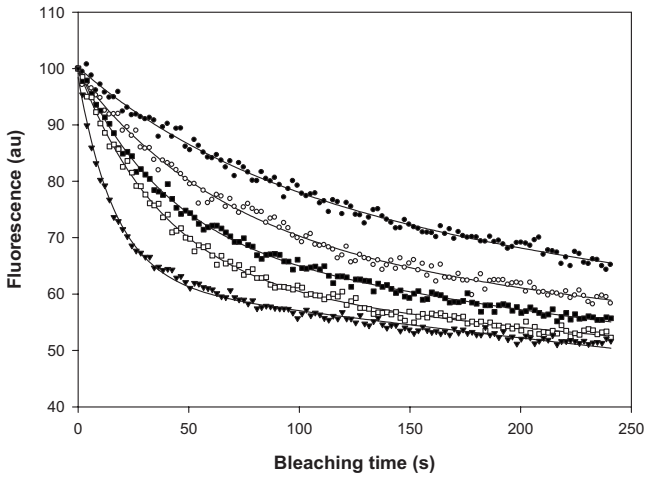

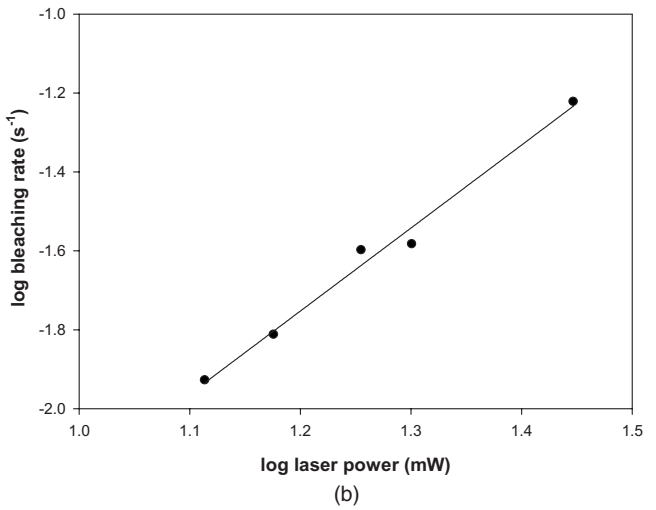

Fig. 3 (a) The fluorescence decay of 2-MDa FITC-dextrans immobilized in acrylamide gel and illuminated with a laser power of 13.8 mW (●), 15.0 mW (○), 18.0 mW (■), 20.0 mW (□), and 28.0 mW (▼). The biexponential function $I(t)=ae^{-bt}+ce^{-dt}$ was fitted to the experimental data to determine the bleaching rate. b is much greater than d and was used as the bleaching rate. (b) The bleaching rates obtained from (a) as a function of laser power.

ROI (radius=1.8 μm), the bleaching profile was well fitted to a distribution corresponding to a Gaussian laser beam [Fig. 4(a)]. Comparing the theoretical and experimental bleaching profile for $R=1.8$ μm (Fig. 5), some discrepancy was found. The theoretical bleaching profile was steeper than the experimental profile, although the profiles showed a great deal of overlap. Based on the good fit of Eq. (5) to the experimental data [Fig. 4(a)] and overlap between the experimental and theoretical profiles, the bleaching profile was approximated to a Gaussian distribution, and the $1/e^2$ radial and axial bleaching radii estimated. When the ROI increased, the bleaching profile became broader in agreement with the simulations. To determine the bleaching radii, the experimental bleaching profile was, as a first approximation, fitted by two functions given by Eq. (5) [Figs. 4(c) and 4(e)]. The edges of the bleaching profiles followed a Gaussian slope, whereas the bottom part was flat and could not be fitted to a Gaussian. Based on two Gaussian functions separated by a distance $2\omega_s$, the radial and axial bleaching radii were estimated. The axial fit was well described by Eq. (5) for all three ROI sizes.

The radial and axial bleaching radii ω_r and ω_z are listed in Table 1. The bleaching radii were essentially identical for the two dextran molecules used, and the data presented in Table 1 are therefore an average of the measurements using the two molecular sizes. The radial radii ω_r increased significantly with increasing ROI, whereas the axial radii ω_z remained equal for all the ROI sizes within experimental error. No significant differences in the bleaching radii were found for the two objectives used.

4.4 *Diffusion during Bleaching*

The characteristic diffusion time $\tau_D=\omega_r^2/8D$ was calculated based on the measured diffusion coefficient for 150-kDa, 500-kDa, and 2-MDa FITC-dextran molecules and the radial bleaching radii. For 150- and 500-kDa dextran molecules in solution, the bleaching time was larger than the characteristic diffusion time, whereas for 2 MDa, the bleaching time and characteristic diffusion time were approximately the same. In gels, the bleaching time was shorter than the characteristic diffusion time, except for 150-kDa dextrans in the lowest concentration of collagen gels (0.24%). According to Meyvis et al.,[17] the characteristic diffusion time should be 15 times longer than the bleaching time, and that was not the case in our experimental setup.

Diffusion during bleaching was therefore determined by imaging the fluorescence intensity profile immediately (0.1 ms) after bleaching of 150-kDa, 500-kDa, and 2-MDa FITC-dextrans in PBS and 0.24% collagen gel. ROI sizes of 1.8 and 3.6 μm were used. Equation (5) was fitted to the intensity profiles to obtain ω_r and β. This was done for ten independent profiles to estimate the average value of ω_r and β. These average values obtained for dextran molecules in solutions and collagen gels were compared with the corresponding average values for dextran molecules immobilized in gels. The bleaching profiles obtained in solution using ROI 1.8 μm are shown in Fig. 6. In solution and immobilized gels, ω_r was statistically equal for all molecules tested when using ROI 1.8 μm. However, β decreased with decreasing molecule size, indicating that some diffusion occured during bleaching. For immobilized gels, $\beta=0.86\pm0.16$, while for dextrans in solution, β was reduced to 0.51 ± 0.12, 0.44 ± 0.11, and 0.27 ± 0.07 for dextran sizes 2 MDa, 500 kDa, and 150 kDa, respectively. In collagen gels, β was only reduced for 150 kDa to 0.39 ± 0.10. When increasing the ROI to 3.6 μm, approximately the same bleaching profiles were obtained in solution and in immobilized gels, both with respect to ω_r and β (in solution $\omega_r=4.40\pm0.77$ μm and $\beta=0.55\pm0.16$). This suggests that although the bleaching time increased with increasing ROI, the recovery time will also increase, and no significant diffusion took place during the bleaching process.

4.5 *Measurements of Diffusion in Solution*

The diffusion coefficients for IgG and dextran molecules of various sizes in solution were determined for the smallest ROI used (1.8 μm). The experimentally estimated radial and axial bleaching radii were substituted in Eq. (8), which was fitted to

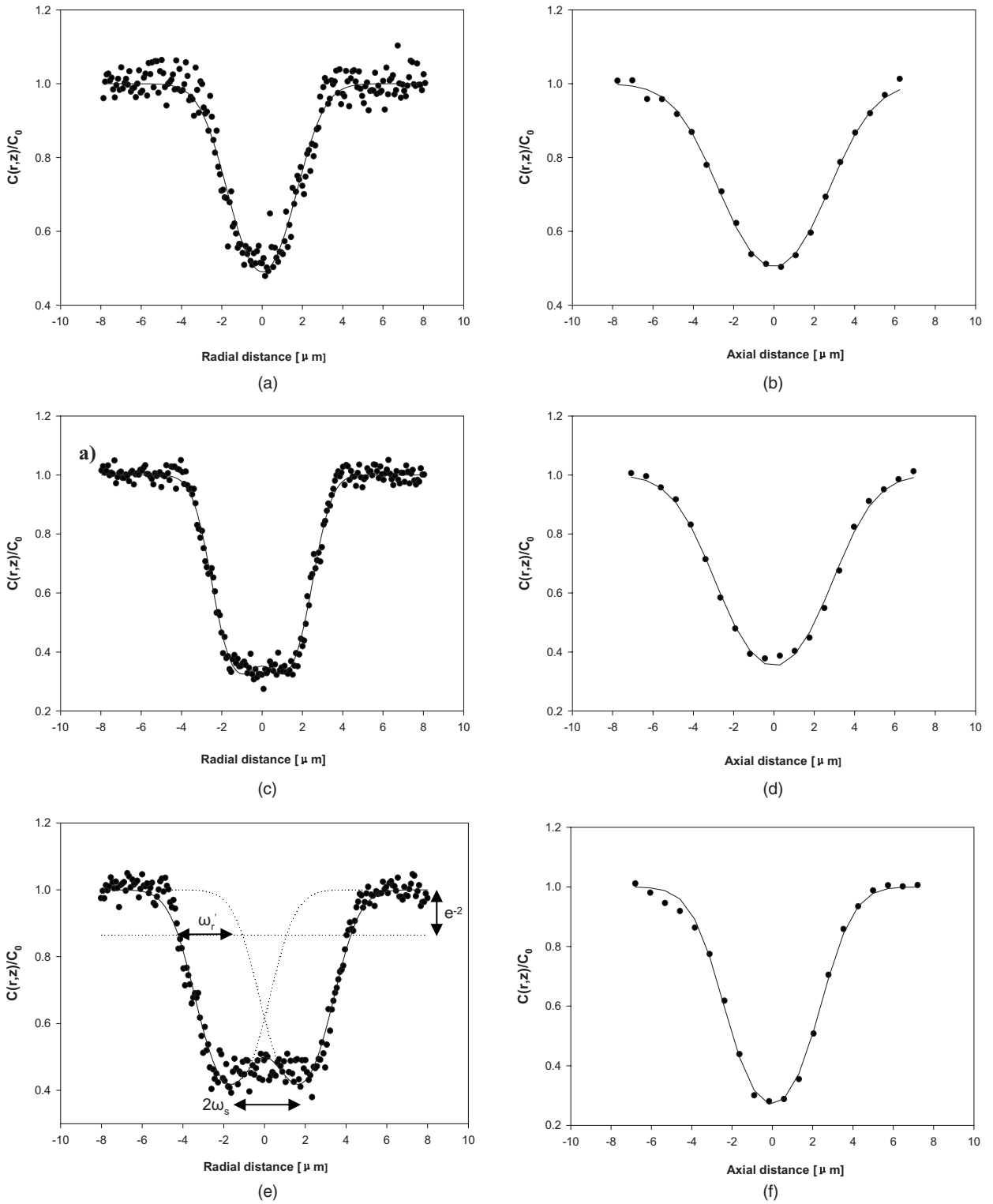

Fig. 4 Radial and axial fluorescence intensity profiles of different sized bleached ROIs using 2-MDa FITC-dextrans immobilized in acrylamide gel. The profiles are the average of ten independent profiles. (a) and (b) ROI radius 1.8 μm, (c) and (d) ROI radius 2.7 μm, and (e) and (f) ROI radius 3.6 μm. Dots represent the experimental data, and solid lines represent the fit from Eq. (5). The fluorescence intensity is normalized to the intensity of the unbleached pixels. (e) shows the two Gaussian profiles separated a distance $2\omega_s$, each with $1/e^2$ radius ω_r'.

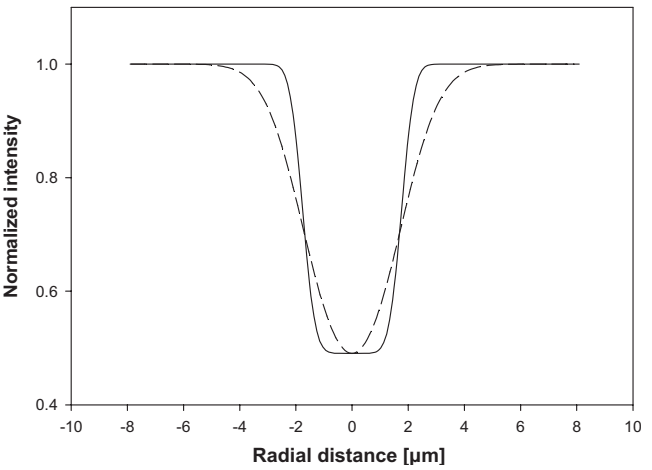

Fig. 5 Simulated bleach light distribution from Eq. (2) with R =1.8 μm and ω_r=1 μm (solid line), and experimental bleach profile R=1.8 μm (broken line).

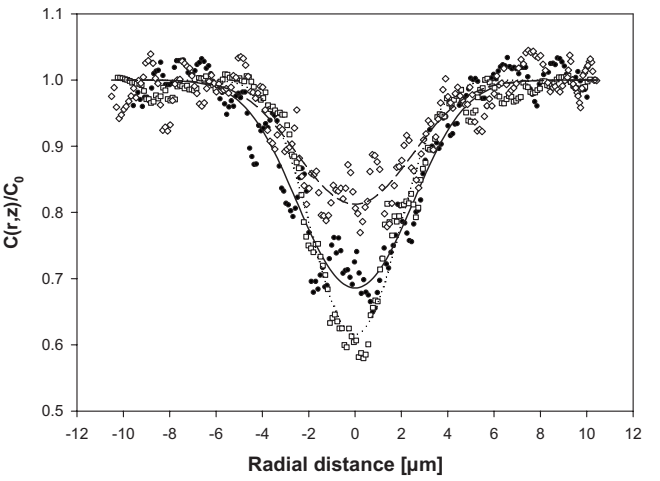

Fig. 6 Fluorescence intensity profiles immediately (0.1 ms) after bleaching of 150 kDa (◇,—), 500 kDa (●,—), and 2 MDa (□,···) dextrans in solution, using a ROI of 1.8 μm. The profiles are the average of ten independent profiles. Equation (5) has been fitted to the experimental intensity profiles. The fluorescence intensity is normalized to the intensity of the unbleached pixels.

the experimental recovery curve to obtain the diffusion coefficient. Our experimental diffusion coefficients were compared to the literature and theoretical values. The theoretical diffusion coefficient was determined based on the Stokes-Einstein equation:

$$D = kT/6\pi\eta R_h, \tag{9}$$

where R_h is the hydrodynamic radius, η the viscosity, k the Bolzmann constant, and T the absolute temperature. The hydrodynamic radii were found from previously published data.[18,19]

A typical recovery curve showing the experimental data and the fit based on Eq. (8) are presented in Fig. 7. The measured diffusion coefficients as well as the literature and theoretical values are presented in Table 2. The diffusion coefficients previously reported are based on 2-D FRAP measurements using a conventional fluorescence microscope with a stationary laser or CLSM with a scanning laser. Within experimental error and the fact that some diffusion occurs during bleaching, the values reported here using two-photon excitation laser scanning microscopy are in accordance with 2-D FRAP measurements. The theoretical values for the larger dextran molecules are somewhat smaller than the experimental values, probably due to the hydrodynamic radii used. In the literature these radii vary, and we chose to refer to values from only two different papers.[18,19] The diffusion coefficient decreased nonlinearly with increasing molecular weight. The experimental data can be described by a power law expression.[20]

Table 1 Experimental values of ω_r and ω_z determined as the $1/e^2$ radii of the bleaching profile of immobilized FITC-dextran molecules.

	C-Apochromat 40×/1.2 W		C-Achroplan 40×/0.18 W	
ROI rad (μm)	ω_r (μm)	ω_z (μm)	ω_r (μm)	ω_z (μm)
1.8	2.66±0.17	3.87±0.31	—	—
2.7	3.18±0.08	4.03±0.50	—	—
3.6	4.41±0.26	3.76±0.27	3.82±0.51	4.23±0.55

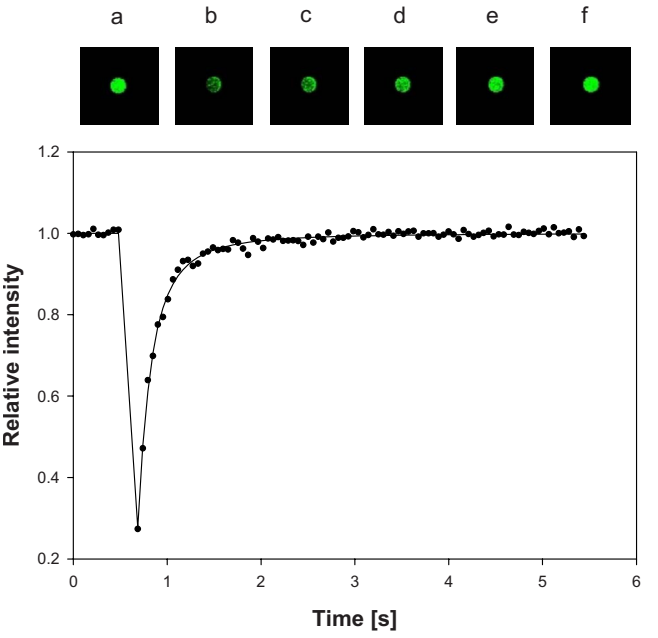

Fig. 7 Typical fluorescence intensity, bleaching, and recovery curve for 2-MDa FITC-dextran in solution. The solid line represents the fit [Eq. (8)] and the dots represent the experimental data. The images show the fluorescence intensity in the bleached ROI at different times: (a) before bleaching, (b) 0.1 ms after bleaching, (c), (d), and (e) during recovery, and (f) full recovery.

Table 2 Diffusion coefficients at 20 °C for various dextran molecules and IgG in PBS. Experimental data are compared to literature values (with standard deviations when reported) and theoretical values calculated from the hydrodynamic radius R_h of the molecule and the Stokes-Einstein equation. n is the number of measurements for each case.

M_W [kDa]	R_h [Å]	D_{exp} [10^{-8} cm^2/s]	D_{lit} [10^{-8} cm^2/s]	Reference	D_{theo} [10^{-8} cm^2/s]
40	47.8	45.0±1.6	46.3±4.6	19	44.8
		(n=10)	51.5±2.3	4	
150 (IgG)	52.9	36.7±11.6	40.0±5.0	30	40.6
		(n=59)	45.0	31	
150	90.7	23.2.0±5.1	18.8±0.17	3	23.7
		(n=20)	35.0	32	
500	159.0	22.4±2.6	23.2±1.1	4	13.5
		(n=30)	22.0	32	
2000	268.9	12.9±3.6	6.4±0.09	3	8.0
		(n=20)	15.0	32	
			9.6±1.0	23	

$$D = a(M_W)^{-b}. \tag{10}$$

This analysis was carried out for the linear dextran molecules, and Eq. (10) was fitted to the experimental data presented in Fig. 8. This resulted in $a=1.3\cdot10^{-5}$ and $b=0.32$.

Although the larger ROIs introduce non-Gaussian bleaching profiles, Eq. (8) was used to determine the diffusion coefficient to estimate the deviation from the diffusion coefficient obtained for the smallest ROI. The appropriate radial and axial bleaching radii were inserted into Eq. (8). No significant difference in the diffusion coefficients was found for the different ROIs, except for 40-kDa dextran (Table 3). This indicates that Eq. (8) may be used to determine the diffusion coefficient for larger molecules, even for the non-Gaussian bleaching profiles obtained using a scanning radius up to 3.6 μm.

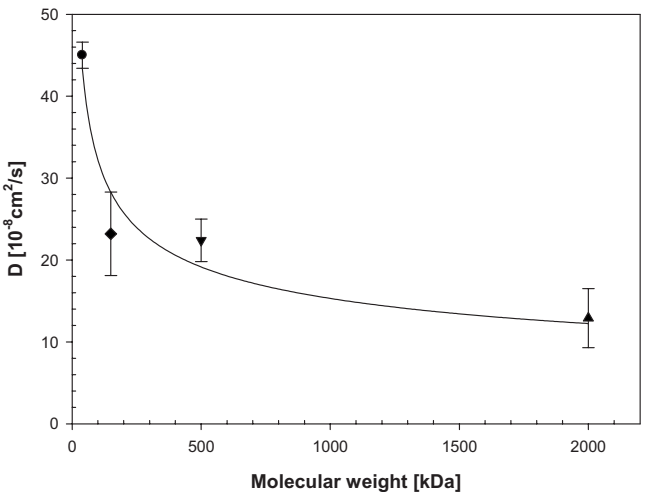

Fig. 8 Diffusion coefficients of 40-kDa (●), 150-kDa (♦), 500-kDa (▼), and 2-MDa (▲) dextrans. The vertical bars indicate the standard deviation, and the solid line indicates the fit $D=1.3\cdot10^{-5}\ M_W^{-0.32}$. The correlation index $R^2=0.93$.

4.6 *Comparing Diffusion in Solution, Gels, and Tissue*

Diffusion of 150-kDa and 2-MDa dextran molecules in solution were compared with biologically more relevant systems such as collagen and gelatin gels, multicellular spheroids, and tumors growing in dorsal window chambers [Fig. 9(a)]. The FRAP measurements and estimation of diffusion coefficients were carried out as for solution. In spheroids and tumors, the ROIs were placed in the extracellular matrix to determine interstitial diffusion. The diffusion coefficient decreased as the complexity of the system and collagen concentration increased. The diffusion coefficient was reduced for all the sys-

Table 3 Diffusion coefficient [10^{-8} cm^2/s] at 20 °C in PBS for various dextran molecules using three different ROIs.

Dextran size	ROI 1.8 μm	ROI 2.7 μm	ROI 3.6 μm
40 kDa	45±1.6	37.8±1.2	35.1±0.6
150 kDa	23.2±5.1	20.8±3.9	24.8±2.4
500 kDa	22.4±2.6	20.4±4.9	21.5±5.3
2 MDa	12.9±3.6	12.9±2.9	14.6±4.1

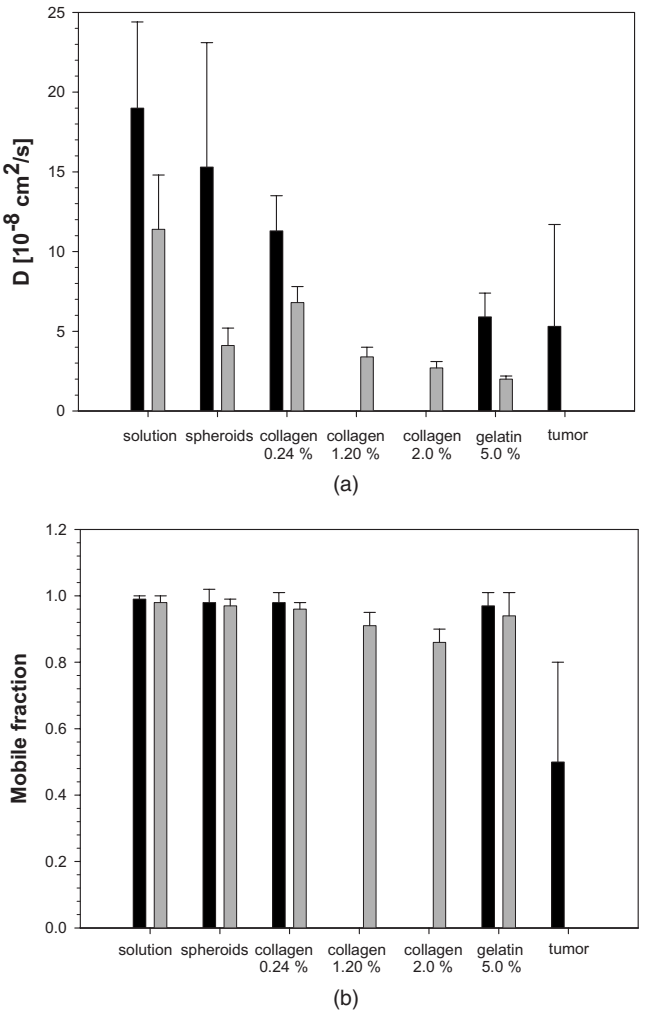

Fig. 9 Diffusion coefficients (a) and mobile fractions (b) of 150-kDa (black columns) and 2-MDa (gray columns) dextrans in solution, collagen gels, gelatin gels, spheroids, and tumors. Each value is the mean of 20 to 90 measurements. Standard deviations are indicated as error bars.

tems compared to values in solution. Diffusion of 150-kDa dextrans was reduced 20 to 60% in spheroids and gels, and more than 70% in tumor tissue. The diffusion of 2-MDa dextrans was slower than the case of 150-kDa dextrans, and the diffusion coefficient was reduced 40 to 90% in spheroids and gels compared with solution. This large molecule was not injected into mice, because only a minor fraction of the molecule would be able to cross the capillary wall. The mobility fraction was high (86 to 99%) in all cases except in tumors growing in window chambers, where the mobile fraction was approximately 50% [Fig. 9(b)].

5 Discussion

The results presented demonstrate that 3-D diffusion readily can be measured by FRAP using a two-photon laser scanning microscope. Our semiempirical approach showed that when a high numerical aperture objective is used, the laser may be scanned over an area with a radius less than twice the $1/e^2$ laser radius, and can still maintain an approximately Gaussian bleaching profile. Increasing the scanning area, the bleaching profile could be approximated by a discontinuous step function described as the uniform disk model.[3] The experimental bleaching profiles for small scanning radii were confirmed by the theoretical bleaching profiles obtained by the convolution of the Gaussian laser beam and the circular scanning area, although some discrepancy was observed. The discrepancy is due to the optical components along the light path, the refractive indices of the various media, the scanning procedure, the photobleaching process, the intensity and wavelength of the laser, and diffusion during bleaching. These factors were also shown to broaden the stationary laser beam profile by approximately a factor of 3. The scanning process and laser power used are important for the bleaching profile. In the present work using a commercial system, the scanning speed and repetition rate were set to maximum values, and 100% laser power was used, as this power did not induce excitation saturation. Various bleaching iterations were tested, and ten iterations gave the shortest bleaching time and maximum bleaching. Thus scanning and bleaching conditions were chosen to obtain as fast and effective bleaching as possible.

The estimated bleaching radii are of critical importance for the determination of the diffusion coefficient, as these radii are inserted in Eq. (8) and used to fit to the experimental recovery curve. The radial bleaching radius (ω_r) is approximately equal to the the sum of the ROI radius and the laser beam diameter (1 μm). ω_r increased with increasing ROI, whereas ω_z was independent of ROI within experimental error. The relatively large ω_z may be due to the fact that as long as the scan area is small with relatively close proximity between the partially overlapping rasters/pixels, also a considerable broadening along the axial dimension is expected, depending on residence time in each pixel, laser intensity, etc., and in addition, ω_z depends on any variations in axial positioning of the laser beam during scanning. It should be emphasized that the bleaching radii have to be determined for each objective used, as the size of the bleaching spot increases with decreasing numerical aperture.[16] However, when bleaching a large ROI, the size of the ROI will dominate the effect of the numerical aperture.

Although the largest ROI generated a truncated top-hat bleach profile, we attempted as a first approximation to use Eq. (8) (based on a true Gaussian beam profile) to compare the macromolecular diffusion coefficient in all cases. Surprisingly, all three ROIs tested could be used in determining the diffusion coefficient of larger molecules ($M_w \geqslant 150$ kDa), as Eq. (8) fitted well to the experimental recovery curve and gave the same diffusion coefficient independent of ROI. However, for smaller molecules (40-kDa dextrans), the diffusion coefficient decreased with increasing ROI. The consistence between the diffusion coefficients for the various ROIs indicates that for large molecules, Eq. (8) is not that sensitive to ω_r and may also be used for the truncated bleaching profile. However, a mathematically more correct model would be the uniform disk model described by Braeckmans et al.[3] In the present work we wanted to establish a user-friendly approach to determine the diffusion coefficient, and the model developed by Brown et al.[6] is mathematically simpler. As a rule of thumb we found that this model can be applied when scanning a ROI with radius up to 1.8 times the laser radius.

The FRAP method is based on the assumption that no diffusion takes place during bleaching. For smaller molecules $\leqslant$150 kDa in solution and low density collagen gels, diffusion was found to occur during bleaching, and this is probably also the case in most FRAP experiments reported in solution.[4,21] Braga et al.[4] developed a method to correct for this diffusion using the larger width of the bleaching profile. In our work, no increase in the width of the bleaching profile was observed, only the bleaching parameter was reduced. However, when measuring diffusion of macromolecules in tissue, diffusion is slow and diffusion during bleaching is not likely to cause a problem.

The 3-D diffusion coefficients obtained in solution in the present work were consistent with 2-D diffusion measured by FRAP based on a conventional fluorescence microscope with a stationary laser or a CLSM with a scanning laser, and were also in the same range as the theoretical diffusion coefficient. The large standard errors found in our results are partly due to day-to-day variations in the measurements and partly due to large fluctuations in the fluorescence intensity in the ROIs used to generate the recovery curve, although the fit was good. The diffusion coefficient decreased with increasing molecular weight as reported by others, and the obtained values for the parameters a and b in Eq. (10), which depend on the medium the molecules are diffusing in, are in accordance with earlier investigations in solution.[22,23] Previously published diffusion coefficients show considerable variations, and our results are slightly in the lower range. Thus, 3-D diffusion measurements do not imply a higher diffusion coefficient than 2-D diffusion.

The potential of using two-photon scanning laser excitation and FRAP to measure diffusion in biological tissue was demonstrated in gels, multicellular spheroids and tumors growing in transparent window chambers. Collagen and gelatin gels are well-characterized models for the structural protein network in the extracellular matrix.[12] The transport in the avascular multicellular spheroids is only governed by diffusion, whereas in the vascularized tumor tissue growing in transparent window chambers, both diffusion and convection driven by the pressure gradient take place.[24,25] The values of the diffusion coefficients of the dextran molecules were smaller in all the biological systems tested compared to solution, demonstrating that the extracellular matrix represents a barrier for diffusion. For the larger 2-MDa dextran molecule, the reduction in diffusion coefficient increased with an increasing amount of collagen in the gels. This is in agreement with previously published results of diffusion in tumor tissue, using a conventional microscope and FRAP.[26] The multicellular spheroids and tumor tissue growing in dorsal chambers represent more complex systems than gels, consisting of a structural collagen network embedded in a hydrophilic gel of glycosaminoglycans, as well as cells. The collagen concentration in the spheroids has been measured to 0.05% (unpublished results), and the more retarded diffusion in spheroids compared to 0.24% collagen gels is thus due to the more complex extracellular matrix of the spheroids. The diffusion of the smaller dextran molecule (150 kDa) was also retarded in gels and tissue compared to solution, but not to the same extent as the larger molecule, demonstrating that the extracellular matrix is a more severe barrier for larger molecules. The diffusion coefficient of the 150-kDa dextran molecules in tumors growing in dorsal chambers was approximately three times lower than in spheroids, probably due to the higher level of collagen (0.16%),[27] and the more complex structure of the extracellular matrix.

The recovery curve obtained for tumors in dorsal chambers revealed a high extent of immobilized molecules. This is probably due to interactions between the dextran molecules and the extracellular matrix and tumor cells, as well as steric exclusion and tortuosity of pathways.[26,28] The lack of full recovery of fluorescence into the bleached area may also be due to a fraction of very slowly diffusing molecules. Based on two-photon fluorescence correlation spectroscopy, a two-phase nature of diffusion in tumors has been reported.[29] The slow component had an approximately 2 orders of magnitude lower diffusion coefficient than the fastest component. This slow component is not detectable using FRAP, and would appear as incomplete recovery in the data.

Multiphoton microscopy has several advantages over CLSM regarding the study of thick samples. It is possible to image farther into the tissue due to enhanced light penetration, and detection of the emitted light is more efficient, as no pinhole is required in front of the detector. Combined with tissue growing in transparent window chambers, it provides a valuable tool for molecular imaging *in vivo*, and the present work demonstrates for the first time the potential of FRAP based on two-photon excitation using a scanning laser in studying dynamic transport processes such as diffusion.

Acknowledgment

We thank Asle Sudbø and Magnus Lilledahl for valuable discussions regarding the convolution product and the theoretical bleaching profile, Tore Lindmo for comments on the manuscript, and Martin S. Grønsleth for his programming expertise. The work has been supported by the Norwegian Cancer Society, and The Norwegian Research Council (NanoMat program contract 163529).

References

1. D. Axelrod, D. E. Koppel, J. Schlessinger, E. Elson, and W. Webb, "Mobility measurements by analysis of fluorescence photobleaching recovery kinetics," *Biophys. J.* **16**, 1055–1069 (1976).
2. J. C. G. Blonk, A. Don, H. Vanaalst, and J. J. Birmingham, "Fluorescence photobleaching recovery in the confocal scanning light-microscope," *J. Microsc.* **169**, 363–374 (1993).
3. K. Braeckmans, L. Peeters, N. N. Sanders, S. C. De Smedt, and J. Demeester, "Three-dimensional fluorescence recovery after photobleaching with the confocal scanning laser microscope," *Biophys. J.* **85**, 2240–2252 (2003).
4. J. Braga, J. M. P. Desterro, and M. Carmo-Fonseca, "Intracellular macromolecular mobility measured by fluorescence recovery after photobleaching with confocal laser scanning microscopes," *Mol. Biol. Cell* **15**, 4749–4760 (2004).
5. W. Denk, J. H. Strickler, and W. W. Webb, "2-Photon laser scanning fluorescence microscopy," *Science* **248**, 73–76 (1990).
6. E. B. Brown, E. S. Wu, W. Zipfel, and W. W. Webb, "Measurement of molecular diffusion in solution by multiphoton fluorescence photobleaching recovery," *Biophys. J.* **77**, 2837–2849 (1999).
7. W. R. Zipfel and W. W. Webb, "In vivo diffusion measurements using multiphoton excitation fluorescence photobleaching recovery and fluorescence correlation spectroscopy," in *Methods in Cellular Imaging*, A. Periasamy, Ed., pp. 216–235, Oxford University Press, Oxford, UK (2001).
8. M. Stroh, W. R. Zipfel, R. M. Williams, W. W. Webb, and W. M. Saltzman, "Diffusion of nerve growth factor in rat striatum as determined by multiphoton microscopy," *Biophys. J.* **85**, 581–588 (2003).
9. S. Basu, C. W. Wolgemuth, and P. J. Campagnola, "Measurement of

normal and anomalous diffusion of dyes within protein structures fabricated via multiphoton excited cross-linking," *Biomacromolecules* **5**, 2347–2357 (2004).
10. F. Waharte, C. Brown, S. Coscoy, E. Coudrier, and F. Amblard, "A two-photon FRAP analysis of the cytoskeleton—dynamics in microvilli of intestinal cells," *Biophys. J.* **88**, 1467–1478 (2004).
11. N. Klonis, M. Rug, and I. Harper, "Fluorescence photobleaching analysis for the study of cellular dynamics," *Eur. Biophys. J. Biophys. Lett.* **31**, 36–51 (2002).
12. A. Erikson, H. N. Andersen, S. N. Naess, P. Sikorski, and C. de L. Davies, "Physical and chemical modifications of collagen gels: impact on diffusion," *Biopolymers* **89**, 135–143 (2008).
13. Ø. Fodstad, A. Brøgger, Ø. Bruland, O. P. Solheim, J. M. Nesland, and A. Pihl, "Characteristics of a cell line established from a patient with multiple osteosarcoma, appearing 13 years after treatment for bilateral retinoblastoma," *Int. J. Cancer* **38**, 33–40 (2006).
14. B. Endrich, K. Asaishi, A. Gotz, and K. Messmer, "Technical report—a new chamber technique for micro-vascular studies in unanesthetized hamsters," *Res. Exp. Med. (Berl)* **177**, 125–134 (1980).
15. G. H. Patterson and D. W. Piston, "Photobleaching in two-photon excitation microscopy," *Biophys. J.* **78**, 2159–2162 (2000).
16. R. M. Williams, D. W. Piston, and W. W. Webb, "Two-photon molecular excitation provides intrinsic 3-dimensional resolution for laser-based microscopy and microphotochemistry," *FASEB J.* **8**, 804–813 (1994).
17. T. K. Meyvis, S. C. De Smedt, P. Van Oostveldt, and J. Demeester, "Fluorescence recovery after photobleaching: a versatile tool for mobility and interaction measurements in pharmaceutical research," *Pharm. Res.* **16**, 1153–1162 (1999).
18. J. K. Armstrong, R. B. Wenby, H. J. Meiselman, and T. C. Fisher, "The hydrodynamic radii of macromolecules and their effect on red blood cell aggregation," *Biophys. J.* **87**, 4259–4270 (2004).
19. I. Lang, M. Scholz, and R. Peters, "Molecular mobility and nucleocytoplasmic flux in hepatoma-cells," *J. Cell Biol.* **102**, 1183–1190 (1986).
20. K. A. Granath and B. E. Kvist, "Molecular weight distribution analysis by gel chromatography on sephadex," *J. Chromatogr.* **28**, 69–81 (1967).
21. M. Weiss, "Challenges and artifacts in quantitative photobleaching experiments," *Traffic* **5**, 662–671 (2004).
22. R. K. Jain, "Transport of molecules in the tumor interstitium: a review," *Cancer Res.* **47**, 3039–3051 (1987).
23. A. Pluen, P. A. Netti, R. K. Jain, and D. A. Berk, "Diffusion of macromolecules in agarose gels: comparison of linear and globular configurations," *Biophys. J.* **77**, 542–552 (1999).
24. L. Eikenes, Ø. S. Bruland, C. Brekken, and C. de L. Davies, "Collagenase increases the transcapillary pressure gradient and improves the uptake and distribution of monoclonal antibodies in human osteosarcoma xenografts," *Cancer Res.* **64**, 4768–4773 (2004).
25. L. Eikenes, M. Tari, I. Tufto, O. S. Bruland, and C. de L. Davies, "Hyaluronidase induces a transcapillary pressure gradient and improves the distribution and uptake of liposomal doxorubicin (Caelyx™) in human osteosarcoma xenografts," *Br. J. Cancer* **93**, 81–88 (2005).
26. C. de L. Davies, D. A. Berk, A. Pluen, and R. K. Jain, "Comparison of IgG diffusion and extracellular matrix composition in rhabdomyosarcomas grown in mice versus in vitro as spheroids reveals the role of host stromal cells," *Br. J. Cancer* **86**, 1639–1644 (2002).
27. C. de L. Davies, B. O. Engesaeter, I. Haug, I. W. Ormberg, J. Halgunset, and C. Brekken, "Uptake of IgG in osteosarcoma correlates inversely with interstitial fluid pressure, but not with interstitial constituents," *Br. J. Cancer* **85**, 1968–1977 (2001).
28. A. Pluen, Y. Boucher, S. Ramanujan, T. D. McKee, T. Gohongi, E. di Tomaso, E. B. Brown, Y. Izumi, R. B. Campbell, D. A. Berk, and R. K. Jain, "Role of tumor-host interactions in interstitial diffusion of macromolecules: cranial vs. subcutaneous tumors," *Proc. Natl. Acad. Sci. U.S.A.* **98**, 4628–4633 (2001).
29. G. Alexandrakis, E. B. Brown, R. T. Tong, T. D. McKee, R. B. Campbell, Y. Boucher, and R. K. Jain, "Two-photon fluorescence correlation microscopy reveals the two-phase nature of transport in tumors," *Nat. Med.* **10**, 203–207 (2004).
30. D. A. Berk, F. Yuan, M. Leunig, and R. K. Jain, "Fluorescence photobleaching with spatial fourier-analysis—measurement of diffusion in light-scattering media," *Biophys. J.* **65**, 2428–2436 (1993).
31. P. A. Netti, D. A. Berk, M. A. Swartz, A. J. Grodzinsky, and R. K. Jain, "Role of extracellular matrix assembly in interstitial transport in solid tumors," *Cancer Res.* **60**, 2497–2503 (2000).
32. P. Gribbon and T. E. Hardingham, "Macromolecular diffusion of biological polymers measured by confocal fluorescence recovery after photobleaching," *Biophys. J.* **75**, 1032–1039 (1998).